Reduction of dislocation density in α-Ga_2O_3 epilayers via rapid growth at low temperatures by halide vapor phase epitaxy

Yuichi Oshima[1]*, Hiroyuki Ando[2], and Takashi Shinohe[2]

[1]*Research Center for Electronic and Optical Materials, National Institute for Materials Science, Tsukuba, Ibaraki 305-0044, Japan*

[2]*FLOSFIA Inc., Kyodai-Katsura Venture Plaza, 615-8245 Kyoto, Japan*

E-mail: OSHIMA.Yuichi@nims.go.jp

We demonstrate that the dislocation density in α-Ga_2O_3 epilayers is markedly reduced via rapid growth at low temperatures by halide vapor-phase epitaxy. An α-Ga_2O_3 epilayer grown on (0001) sapphire at a high growth rate of 34 μm/h and a low temperature of 463 °C exhibited a dislocation density of 4×10^8 cm^{-2}, which was approximately 1/100 of that in a conventional film. It is likely that the three-dimensional surface morphology developed during the growth enhanced the bending of the dislocations to increase the probability of pair annihilation. The combination of this technique with thick film growth and epitaxial lateral overgrowth resulted in a further low dislocation density of 1.1×10^7 cm^{-2}.

Corundum-structured α-Ga_2O_3 is a meta-stable phase of α-Ga_2O_3.[1] The thermal stability of α-Ga_2O_3 depends on the film thickness and strain, and the transition temperature to β-Ga_2O_3 is reported to be 500–650 °C.[2,3] α-Ga_2O_3 is an ultra-wide-bandgap semiconductor with an energy gap, E_g, of 5.2–5.3 eV,[4,5] which is the widest among Ga_2O_3 polymorphs. Accordingly, a large critical field can be expected. In addition, α-Ga_2O_3 forms solid solutions with other corundum-structured oxides. For example, it is possible to make α-$(Al_xGa_{1-x})_2O_3$ solid solutions without compositional limitation,[6] in contrast with β-$(Al_xGa_{1-x})_2O_3$. Therefore, α-Ga_2O_3 should allow a higher freedom of band engineering than β-Ga_2O_3. Furthermore, α-Ga_2O_3 can form a hetero-pn junction with isomorphic p-type oxides, such as α-$(Ga_xIr_{1-x})_2O_3$, which virtually lattice matches to α-Ga_2O_3.[7,8] These features make α-Ga_2O_3 an attractive candidate for power-device applications.[9-12]

Despite these advantages, a major drawback of α-Ga_2O_3 is the absence of melt-grown high-quality native substrates, in contrast to the case of β-Ga_2O_3. Accordingly, α-Ga_2O_3 films need to be grown on foreign substrates. Isomorphic sapphire is the most frequently used substrates[4,5,13-15] because large-scale wafers are available at a reasonable price. The dislocation density in a heteroepitaxial α-Ga_2O_3 film is typically of the order of 10^{10} cm^{-2} because of lattice mismatch if no measure is taken to reduce the dislocation density. For example, Kaneko *et al*. reported that the dislocation density in their mist-CVD-grown α-Ga_2O_3 film was as high as 7×10^{10} cm^{-2}.[16] Such a high density of dislocations should degrade the electrical properties of α-Ga_2O_3. Indeed, Son *et al*. experimentally confirmed that α-Ga_2O_3 films with higher dislocation density exhibited lower electron mobility.[17] According to theoretical prediction by Takane *et al.*, the influence of dislocations on the electron mobility in α-Ga_2O_3 should be negligible when the density is 10^7–10^8 cm^{-2} or less.[18] Accordingly, these values should be a target for the reduction of the dislocation density.

Epitaxial lateral overgrowth (ELO) is one of the most frequently reported techniques to decrease the dislocation density in α-Ga_2O_3.[19-23] In the ELO technique, α-Ga_2O_3 islands are selectively grown on the windows of a dielectric mask pattern formed on a seed α-Ga_2O_3

layer (or directly on a sapphire substrate). Each α-Ga_2O_3 island grows vertically and laterally, and the neighboring islands coalesce to form a compact film.[21,23] The dislocation density on the laterally grown areas on the mask is typically as low as 10^7 cm^{-2} because dislocations in the seed layer do not propagate into those areas. However, the dislocation density on the window areas is still as high as that in the seed layer because the dislocations in the seed layer directly propagate into those areas.[23] Thus, a limitation of ELO is that such low-quality areas remain. Although double-ELO process was reported to be effective to reduce the dislocation density on the window areas, the process was not cost-effective since the process required two rounds of photolithography and epitaxial growth.[22]

The use of a super-lattice buffer layer was reported as a maskless method to uniformly reduce the dislocation density.[24] In this technique, a mist-CVD-grown quasi-graded α-$(Al_xGa_{1-x})_2O_3$ super lattice buffer layer was inserted between the α-Ga_2O_3 top layer and the sapphire substrate. As a result, the dislocation density decreased to the order of 10^8 cm^{-2}. However, this technique requires a growth apparatus equipped with an additional gas line to supply the Al precursor, and the growth process is complicated.

In this paper, we demonstrate a maskless method to reduce the dislocation density in an α-Ga_2O_3 epilayer via rapid growth at low temperatures by halide-vapor-phase epitaxy (HVPE). This technique uniformly reduces the dislocation density from 10^{10} to 10^8 cm^{-2} or less without using extra materials or a complicated process unlike the cases of the ELO or super-lattice buffer layers. One of the most advantageous features of HVPE is the rapid growth, with a very high growth rate of α-Ga_2O_3 of over 100 μm/h having been reported.[5,25] We therefore believe this technique is promising to grow thick drift layers for high-performance α-Ga_2O_3-based power devices.

In the present work, we grew the α-Ga_2O_3 epilayers in a lab-made HVPE reactor under atmospheric pressure using O_2 and $GaCl_y$ (y = 1, 3) as the precursors. GaCl was produced by chemical reaction of HCl and metal Ga at 570 °C upstream in the reactor. Additional HCl gas was also supplied to enable rapid growth by suppressing the parasitic gas-phase reaction owing to the conversion of part or all of the GaCl to $GaCl_3$.[25] The HCl partial pressure needs

to be increased with increasing the GaCl supply for rapid growth. N_2 was used as the carrier gas. A (0001) patterned sapphire substrate (PSS) was used[21] because the growth of an α-Ga_2O_3 epilayer with a thickness of approximately 3 μm or more on a flat sapphire substrate (FSS) result in cracking or peeling off of the film.[26] We note that the use of a PSS is not essential in our method from the viewpoint of crystal-quality improvement, and similar results can also be obtained on an FSS.

We investigated the effect of the growth temperature and growth rate on the dislocation density. The α-Ga_2O_3 epilayers were prepared by three-step growth, as described in Table I. Step 1 was to nucleate α-Ga_2O_3 on sapphire at our standard growth temperature of 520 °C with a relatively low growth rate. If the temperature in step 1 is too low, the growth results in an amorphous layer. Then, the growth was interrupted to change the temperature for steps 2 and 3. The duration of the interruption was set according to the temperature difference. Upon restarting the growth after the interruption, the HCl supply needed to be started in prior to the growth precursors to avoid gas-phase parasitic reaction. The HCl pre-flow should also work to etch the film surface grown at step 1. Our aim in step 2 was to perform the pre-flow with a low HCl partial pressure to suppress the etching as possible. If step 2 was skipped, the dislocation density in the subsequent layer grown at step 3 should increase due to the surface residuals produced as a result of rapid etching in the pre-flow process with a high HCl partial pressure, which is necessary for rapid growth. The layer formed in step 3 was the target of our investigation.

Table I. Growth conditions for the three-step growth. *P* denotes the partial pressure of the gas supply.

	Step 1	Interruption	Step 2	Step 3
P(GaCl) [kPa]	0.125	0	0.125	0.125 – 1.00
P(O_2) [kPa]	1.25	1.25	1.25	1.25 – 2.50
P(HCl) [kPa]	0.188	0	0.188	0.188 – 1.25
Temperature [°C]	520	-	463 – 520	
Growth rate [μm/h]	14	-	8.3	8.3 – 80
Thickness [μm]	0.5	-	0.5	10 – 200

After step 3, the sample was etched by HCl gas in the same HVPE reactor to visualize the dislocations as etch pits.[23] The dislocation density was measured as the etch pit density (EPD), which was determined by counting the number of etch pits on four successive surface

areas of 8 μm × 12 μm (approximately 384 μm^2 in total) under SEM. Bright-field plan-view transmission electron microscopy (TEM) was also used to characterize a sample. Three successive surface areas of 2.2 μm × 2.5 μm (approximately 16.5 μm^2 in total) of a sample were observed by TEM to calculate the dislocation density. The surface morphology was observed by SEM. Bright-field cross-sectional TEM was used to investigate the behavior of the dislocations.

Figure 1(a) shows a plan-view SEM image of an α-Ga_2O_3 film with an approximately 10-μm-thick third layer grown at a high growth rate of 34 μm/h and a low temperature of 463 °C. The surface exhibited a rough morphology, which is characteristic of rapid growth at low-temperature. The surface was HCl-gas-etched, and etch pits were visible as black dots. The etch pits were sufficiently isolated to determine the density. The EPD was 4×10^8 cm^{-2}, which was approximately 1/100 of that in conventional α-Ga_2O_3 films. Figure 1(b) shows a plan-view TEM image of the same α-Ga_2O_3 film. The dislocation density was as low as 6×10^8 cm^{-2}. Thus, the remarkable reduction in the dislocation density was confirmed although the TEM value was slightly higher than the EPD. We note that the EPD value should be more accurate than the TEM result because a much larger area was observed, as explained in the experimental details.

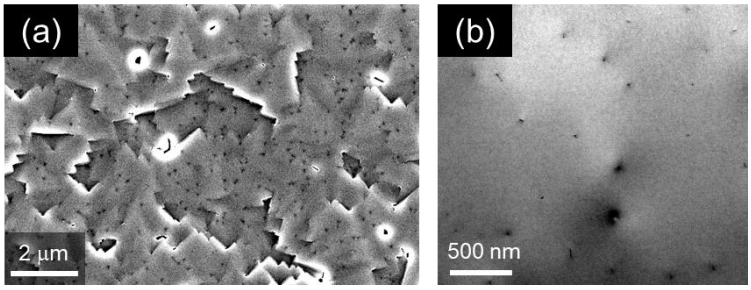

Fig. 1. (a) Plan-view SEM image and (b) plan-view TEM image of an α-Ga_2O_3 epilayer grown at a growth rate of 34 μm/h and a temperature of 463 °C.

Figure 2(a) is a cross-sectional TEM image of the sample shown in Fig. 1, including the substrate boundary to the top surface. A steep decrease in the dislocation density was observed at a thickness of a few micrometers. The magnified image (Fig. 2(b)) revealed that the steep decrease took place in step 3. Bending of dislocations and dislocation loops were also observed. Figure 2(c–e) exhibits the surface morphologies at different growth stages. At

the end of step 1 (Fig. 2(e)), the surface was smooth except for a bump on the PSS. At the end of step 2 (Fig. 2(d)), surface roughening was observed. During step 3 (Fig. 2(c)), three-dimensional (3D) growth was further promoted. The 3D growth probably occurred because of the destabilization of the (0001) plane at low temperature[19] triggered by the rapid growth, whereby surface migration of the growth species should be suppressed. In general, a dislocation line tends to be perpendicular to the free surface to minimize the elastic strain energy. Accordingly, a dislocation line bends to follow the surface when the surface angle changes. Such bending was reported for ELO-grown α-Ga_2O_3 and GaN.[19,27,28] The bending mechanism in the present work should be similar. It is likely that the bending increased the probability of pair annihilation, and resulted in the reduction in the dislocation density.

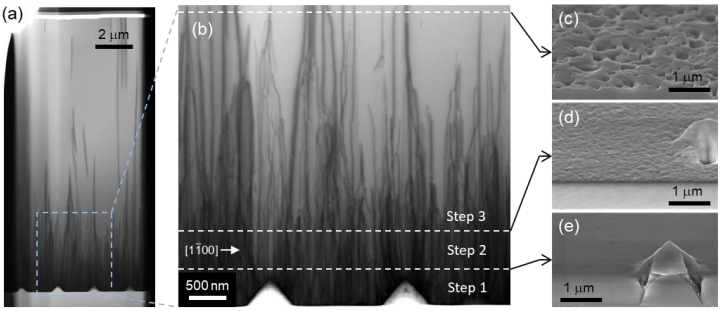

Fig. 2. (a) Cross-sectional TEM image of the α-Ga_2O_3 epilayer shown in Fig. 1. (b) Magnified image of (a). (c, d) Bird's-eye-view SEM image of the surface at each growth step.

To clarify the effect of growth temperature on the dislocation density, α-Ga_2O_3 epilayers were grown at different temperatures with a fixed precursor supply in step 3. GaCl, O_2, and HCl were supplied with partial pressures of 0.75, 2.5, and 1.25 kPa, respectively. The growth rate under these growth conditions was 52 μm/h at 463 °C. We note that the growth rate increased with increasing temperature, reaching 74 μm/h at 520 °C. This is probably because the growth was in the transient regime of mass-transport limited and reaction-limited growth. The growth time was set such that the thickness of the third layer was approximately 10 μm. Figure 3(a) shows the EPD as a function of growth temperature. Surface SEM images of selected samples are also shown. The EPD monotonically decreased with decreasing temperature. We note that the EPD of a sample grown at the standard temperature of 520 °C could not be calculated because the dislocation density was too high. The increase in the surface roughness at low temperature supports the reduction mechanism described above.

To clarify the effect of growth rate on the dislocation density, α-Ga_2O_3 epilayers were grown at different growth rates at a fixed low temperature of 478 °C in step 3. The film thickness of the third layer was approximately 10 μm. Figure 3(b) shows the EPD as a function of growth rate. Surface SEM images of selected samples are also shown. The EPD was countable even at the lowest growth rate of 8.3 μm/h, at which it was 1.6×10^9 cm^{-2}. The EPD further decreased at 37 μm/h but gradually increased at higher growth rates. The samples with smaller EPD exhibited rougher surfaces as expected. We note that the surface of the sample with a growth rate of 80 μm/h was smoother than that with a growth rate of 37 μm/h sample. We speculate that this was because of the increase in the effective growth temperature owing to the heat of reaction of GaCl and HCl to produce $GaCl_3$.

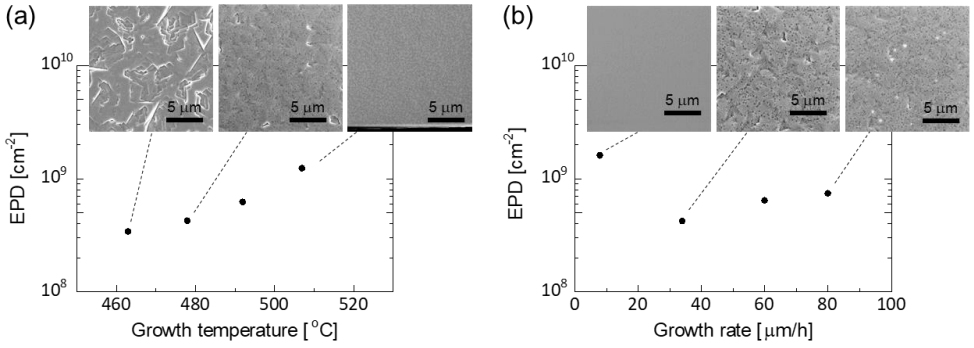

Fig. 3. (a) Dislocation density in α-Ga_2O_3 epilayers as a function of growth temperature. Plan-view SEM images of the selected samples are also shown. (b) Dislocation density in α-Ga_2O_3 epilayers as a function of growth rate. Plan-view surface SEM images of the selected samples are also shown.

For GaN, the dislocation density is known to decrease during thick film growth even if the surface is smooth.[29,30] This is because dislocations with Burgers vector of opposite signs gradually approach each other owing to the attractive force and finally react to form a dislocation loop. In the present work, thick film growth was combined with rapid growth at a low temperature to further decrease the dislocation density. In step 3 of the growth, GaCl, O_2, and HCl were supplied with partial pressures of 1.00, 2.5, and 1.25 kPa, respectively, and the growth temperature was 463 °C. The growth rate was 70 μm/h under these growth

conditions. Figure 4 (a–c) shows SEM images of the etched surface of the thick α-Ga_2O_3 epilayers. The EPD decreased with increasing thickness, reaching 1.5×10^8 cm^{-2} at 200 μm (Fig. 4(e)).

ELO was combined with thick film growth to further decrease the dislocation density. α-Ga_2O_3 was grown at 463 °C on a 3-μm-thick (0001) α-Ga_2O_3 template with a striped TiO_x mask pattern along $[1\bar{1}00]$. The widths of the mask and window were 5 and 5 μm, respectively. The details of the process are described elsewhere.[21,23] The three-step growth was performed using the same gas-supply conditions as those for the samples shown in Fig. 4(a–c). The film thickness was 140 μm excluding the template layer. Figure 4(d) shows a plan-view SEM image of the etched sample. In contrast with the conventional ELO sample, high-dislocation density areas did not exist, although the surface still exhibited a rough morphology that originated from stripe coalescence. The EPD was as low as 1.1×10^7 cm^{-2}. We attribute the good uniformity to the reduction of dislocation density on the windows via the rapid growth at low temperature, and the dispersion of the dislocations (including those newly formed at the coalesced boundaries) during the thick film growth after coalescence owing to the repulsive interaction between dislocations with Burgers vectors of the same sign. We note that the dislocation density on the window regions was much lower than those of the thick films with similar thickness. This is probably because the faceting was clearer as shown in Fig. 5. V-shaped facets were observed on the top of the stripes with high density, although the reason for such morphological difference from the plain films is under investigation. It is also likely that the V-shaped facets swept the surface like waves as the growth proceeds[14] to further increase the possibility of dislocation bending.

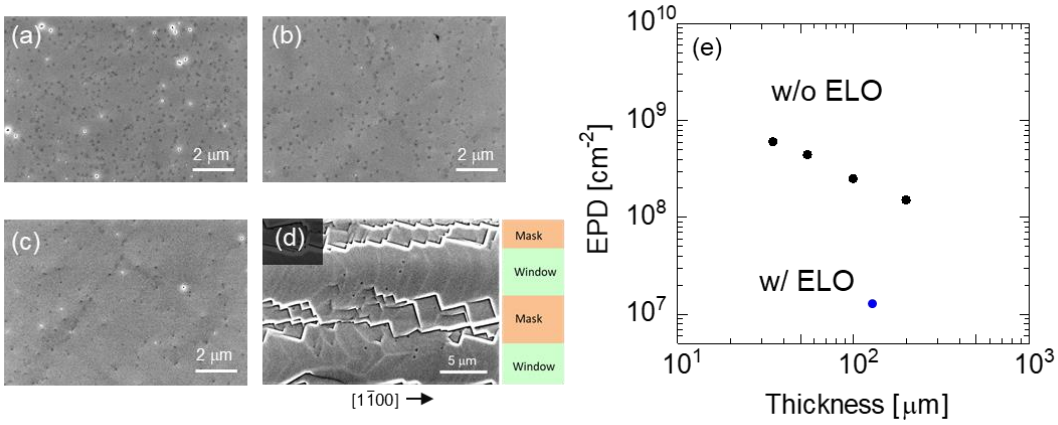

Fig. 4. (a–c) Plan-view SEM images of α-Ga_2O_3 epilayers with thicknesses of 35, 100, and 200 μm, respectively. (d) Plan-view SEM images of an α-Ga_2O_3 epilayer prepared using the ELO technique with a thickness of 140 μm. (e) Dislocation density in the samples in (a–d) as a function of film thickness.

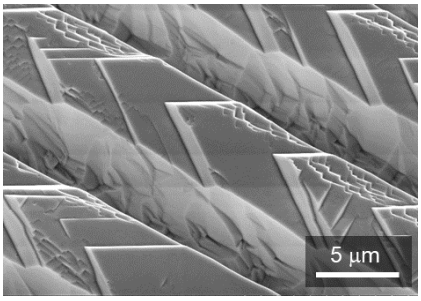

Fig. 5. Bird's-eye-view SEM images of α-Ga_2O_3 stripes grown using the same recipe with that for the sample shown in Fig. 1.

In summary, we demonstrated that rapid growth at low temperatures by HVPE effectively reduces the dislocation density in α-Ga_2O_3 epilayers without leaving high-dislocation-density areas, in contrast with conventional ELO. We attribute the reduction of the dislocation density to the enhancement of pair annihilation by the bending triggered by the 3D growth. The dislocation density of an α-Ga_2O_3 epilayer grown by this method was 4×10^8 cm^{-2}, which was approximately 1/100 of that in a film grown without measures against dislocations. The combination of this method with ELO and thick film growth further reduced the dislocation density to 1.1×10^7 cm^{-2}, to which the carrier scattering should be negligible even for a very low carrier concentration of 1×10^{15} cm^{-2}.[18)]

Acknowledgement

Part of this work was supported by the Innovative Science and Technology Initiative for Security (JPJ004596), ATLA, Japan.

References

1) R. Roy, V. G. Hill, and E. F. Osborn, J. Am. Chem. Soc. **74**, 719 (1952).
2) S. Lee, Y. Ito, K. Kaneko, and S. Fujita, Jpn. J. Appl. Phys. **54**, 030301 (2015).
3) R. Jinno, K. Kaneko, and S. Fujita, AIP Advances **10**, 115013 (2020).
4) D. Shinohara and S. Fujita, Jpn. J. Appl. Phys. 47, 7311-7313 (2008).
5) Y. Oshima, E. G. Villora, and K. Shimamura, Appl. Phys. Express **8**, 055501 (2015).
6) S. Fujita and K. Kaneko, J. Cryst. Growth 401, 588-592 (2014).
7) K. Kaneko, S. Fujita, and T. Hitora, Jpn. J. Appl. Phys. 57, 02CB18 (2018).
8) K. Kaneko, Y. Masuda, S. Kan, I. Takahashi, Y. Kato, T. Shinohe, and S. Fujita, Appl. Phys. Lett. **118**, 102104 (2021).
9) M. Oda, R. Tokuda, H. Kambara, T. Tanikawa, T. Sasaki, and T. Hitora, Appl. Phys. Express **9**, 021101 (2016).
10) News release from FLOSFIA and Kyoto university, July 13, 2018 (https://flosfia.com/struct/wp-content/uploads/79cd9d2dfa54a771f642e008cc4f9cb0.pdf).
11) Y. Jeong, J. Park, M. Yeom, I. Kang, J. Yang, H. Kim, D. Jeon, and G. Yoo, Appl. Phys. Express **15**, 074001 (2022).
12) T. Shinohe, Proceedings of the 2022 International Power Electronics Conference (IPEC-Himeji 2022- ECCE Asia), Himeji, Japan, page 627-631 (2022).
13) Z. Cheng, M. Hanke, P. Vogt, O. Bierwagen, and A. Trampert, Appl. Phys. Lett. **111**, 162104 (2017).
14) Y. Oshima, S. Yagyu and T. Shinohe, J. Appl. Phys. **130**, 175304 (2021).
15) A. F. M. A. U. Bhuiyan, Z. Feng, H.-L. Huang, L. Meng, J. Hwang, and H. Zhao, APL Mater. **9**, 101109 (2021).
16) K. Kaneko, S. Fujita, and T. Hitora, Jpn. J. Appl. Phys. **57** 02CB18 (2018).
17) H. Son, Y. Choi, J. Park, B. Ryu, and D. Jeon, ECS Journal of Solid State Science and Technology **9**, 055005 (2020).
18) H. Takane, H. Izumi, H. Hojo, T. Wakamatsu, K. Tanaka and K. Kaneko, J. Mater. Res.

38, 2645 (2023).

19) Y. Oshima, K. Kawara, T. Shinohe, T. Hitora, M. Kasu, and S. Fujita, APL Mater. **7**, 022503 (2019).
20) R. Jinno, N. Yoshimura, K. Kaneko, and S. Fujita, Jpn. J. Appl. Phys. **58** 120912 (2019).
21) Y. Oshima, K. Kawara, T. Oshima, M. Okigawa, and T. Shinohe, Jpn. J. Appl. Phys. **59** 025512 (2020).
22) K. Kawara, Y. Oshima, M. Okigawa, and T. Shinohe, Appl. Phys. Express **13**, 075507 (2020).
23) Y. Oshima, S. Yagyu, T. Shinohe, J. Cryst. Growth **576**, 126387 (2021).
24) R. Jinno, T. Uchida, K. Kaneko, and S. Fujita, Appl. Phys. Express **9**, 071101 (2016).
25) Y. Oshima, K. Kawara, T. Oshima, M. Okigawa, and T. Shinohe, Semicond. Sci. Technol. **35**, 055022 (2020).
26) M. Oda, K. Kaneko, S. Fujita, and T. Hitora, Jpn. J. Appl. Phys. **55**, 1202B4 (2016).
27) A. Usui, H. Sunakawa, A. Sakai and A. Yamaguchi, Jpn. J. Appl. Phys. **36**, L899 (1997).
28) A. Sakai, H. Sunakawa and A. Usui, Appl. Phys. Lett. **73**, 481 (1998).
29) K. Fujito, S. Kubo, H. Nagaoka, T. Mochizuki, H. Namita, S. Nagao, J. Cryst. Growth **311**, 3011-3014 (2009).
30) H. Fujikura, T. Konno, T. Suzuki, T. Kitamura, T. Fujimoto, and T. Yoshida, Jpn. J. Appl. Phys. **57**, 065502 (2018).